JREE: Vol. 13, No. 1, (Winter 2026) 85-93

Journal of Renewable Energy and Environment

Journal Homepage: www.jree.ir

Materials and Energy Research Center

MERC

Research Article

Improving the CO_2 Adsorption Capacity and Selectivity with ZIF-67: A Study on Synthesis Factors and Structural Parameters

Fatemeh Behzadi[a], Ali Asghar Ghoreyshi[a], Fatemeh Aghili[b]*

[a] Department of Chemical Engineering, Babol Noshirvani University of Technology, P. O. Box: 47148-71167, Babol, Iran.
[b] Department of Chemical Engineering, Faculty of Engineering and Technology, University of Mazandaran, P. O. Box: 47416-13534, Babolsar, Iran.

PAPER INFO

Paper history:
Received: 07 March 2025
Revised: 03 October 2025
Accepted: 12 November 2025

Keywords:
CO_2 Adsorption,
ZIF-67,
Synthesis,
CO_2/N_2 Separation

ABSTRACT

In this research, ZIF-67 was used for CO_2 capture and its separation from flue gas. To improve the CO_2 adsorption capacity, the synthesis factors of ZIF-67 were optimized. For this purpose, the molar ratios of salt to ligand, salt to solvent, and the synthesis temperature were investigated. The optimum sample, synthesized at room temperature, was prepared with a 1:4:741 molar ratio corresponding to salt, ligand, and solvent, respectively. After comparing the textural properties of the samples, the highest surface area (2285 m^2/g) and the lowest pore diameter (1.19 nm) were obtained for the optimum sample, showing good performance for CO_2 adsorption. The optimized ZIF-67 adsorbed 0.94 mmol/g of CO_2 at 293 K and 1 bar. Furthermore, the sample was used for N_2 adsorption at different temperatures, and the highest CO_2/N_2 selectivity was measured as 5.86 at 313 K. The synthesized ZIF-67 retained more than 93% of its efficiency after five adsorption–desorption cycles, which is a suitable feature for industrial applications in CO_2 capture.

https://doi.org/10.30501/jree.2025.508558.2285

1. INTRODUCTION

Global warming has led to severe environmental consequences, such as rising sea levels and glacier melting, making it a worldwide concern in which carbon dioxide (CO_2) plays a major role (Yamasaki, 2003). The combustion of fossil fuels is recognized as one of the main sources of CO_2 emissions (Li et al., 2025; Bheeram et al., 2023). Over the past years, with rapid population growth and industrial development, the consumption of fossil fuels has significantly increased. Consequently, the atmospheric concentration of CO_2 has also increased. Therefore, efficient approaches should be considered to control CO_2 emissions. Generally, three technologies have been proposed for carbon capture, namely pre-combustion, oxy-fuel combustion, and post-combustion. Among them, post-combustion capture is considered a practical technology because many emission sources can be adapted to it. So far, different methods for post-combustion capture have been proposed, including membrane separation, cryogenics, absorption, and adsorption by porous solid sorbents (Olajire, 2010). Due to its simple operational conditions, low cost, and high yield, adsorption has attracted much attention (Ahmed et al., 2017; Kim et al., 2012).

Different adsorbents have been investigated for CO_2 adsorption, including Metal–Organic Frameworks (MOFs) and carbon nanotubes (Wei et al., 2025; Anbia & Hoseini, 2012). MOFs are recognized as porous materials that have received considerable attention owing to their unique textural properties. These adsorbents have been widely used for gas adsorption and separation. MOFs can be considered favorable candidates for CO_2 capture because they possess desirable features such as high specific surface area, suitable pore size, and large pore volume. Structurally, they are composed of metal clusters and organic ligands. The diversity of these metal clusters and organic ligands leads to a wide variety of MOF structures.

Recently, a subfamily of MOFs known as Zeolitic Imidazolate Frameworks (ZIFs) has emerged. ZIFs are constructed from metal ions (Co^{2+}, Zn^{2+}) and imidazolate linkers, and their structure is similar to that of zeolites. Since ZIFs simultaneously exhibit the characteristics of both MOFs and zeolites, they are expected to possess distinct features, including ultrahigh surface area, unique micropores, high porosity, and tunable pore diameter (Fairen-Jimenez et al., 2011; Wang et al., 2011). Owing to these properties, ZIFs are appropriate candidates for CO_2 adsorption. One of them is ZIF-67 (Co $(mIm)_2$) constructed by metal cations (Co^{2+}) and 2-methyl imidazolate anions and shows a structure similar to ZIF-8 (Yang et al., 2018). ZIF-67 can be applied in gas adsorption, particularly for CO_2 adsorption, as well as in catalysis and sensors. The pore sizes of ZIF-67 typically range between 1 and

*Corresponding Author's Email: f.aghili@umz.ac.ir (F. Aghili)

URL: https://www.jree.ir/article_234111.html

Please cite this article as: Behzadi, F., Ghoreyshi, A. A., & Aghili, F. (2026). Improving the CO2 Adsorption Capacity and Selectivity with ZIF-67: A Study on Synthesis Factors and Structural Parameters, *Journal of Renewable Energy and Environment (JREE)*, 13(1), 85-93. https://doi.org/10.30501/jree.2025.508558.2285

2 nm, and its pore volume is approximately 0.7 cm^3/g. The particle size of ZIF-67 varies from 78 to 385 nm. ZIF-67 can remain stable up to 500 °C, indicating high thermal stability. Yang et al (Yang et al., 2018) proposed LDH@ZIF-67 for CO_2 adsorption, where the composite consisted of Co–Al LDH (Layered Double Hydroxides) and ZIF-67. The surface area and pore volume of LDH@ZIF-67 were reported as 1196.5 m^2/g and 0.55 cm3/g, respectively, which are higher than those of Co–Al LDH. They demonstrated that ZIF-67 significantly improved the composite's CO_2 adsorption performance. Bhreeram et al. (Bheeram et al., 2023) doped Ni^{2+} ions into ZIF-67 as an adsorbent for CO_2 adsorption. Three doping levels (10%, 25%, and 75%) were prepared and their performances were investigated. The study revealed that doping ZIF-67 with 75% Ni^{2+} ions resulted in the highest specific surface area of 1364 m^2/g. The CO_2 adsorption capacity of Ni@ZIF-67 was reported as 33.65 mg/g, while ZIF-67 alone exhibited a capacity of 24.76 mg/g. Hamami et al. (Hammi et al., 2023) employed an in-situ growth approach to synthesize composite ZIF-67/ chitosan beads. The resulting composite exhibited a specific surface area of up to 1200 m^2/g. The study reported an adsorption capacity of 1.21 mmol/g for CO_2 at 273 K. Missaoui et al. (Missaoui et al., 2024) introduced a green, solvent-free synthesis method for SOD-ZIF-67. Their study revealed that the sample with a molar ratio of 2:1 (cobalt:ligand) exhibited the highest surface area and pore volume, 1923 m^2/g and 0.72 cm^3/g, respectively. The CO_2 adsorption capacity of this sample reached 2.08 mmol/g at 298 K and 100 kPa. Zhao et al. (Zhao et al., 2025) proposed a synthesis method for amino-functionalized ZIF-67. Based on their findings, the maximum CO_2 adsorption capacity of 191.45 cm^3/g at 298 K and 1 MPa was achieved for ZIF-67-NH_2-24h. In this sample, the amino groups significantly reduced the CO_2 adsorption energy, thereby increasing CO_2 selectivity.

It is worth mentioning that CO_2 is more attracted to adsorbents with low pore diameter, high pore volume, and high specific surface area (Lai et al., 2021). By controlling the synthesis parameters of ZIF-67, it is possible to adjust the adsorbent textural properties. Lai et al. (Lai et al., 2014) investigated the effect of synthesis conditions, including the molar ratio of solvent, synthesis duration, and pH, on the textural properties of ZIF-8. The optimized adsorbent was prepared within 60 minutes at pH 7.6 and a 1:7.9:86.7 molar ratio of salt, ligand, and solvent, respectively. The surface area and pore volume of the optimized adsorbent were reported as 1344 m^2/g and 0.68 cm3/g, respectively. Under these synthesis conditions, the adsorbent achieved a CO_2 adsorption capacity of 0.53 mmol/g at 298 K.

In contrast to previous studies that focused on CO_2 adsorption by either pristine or modified ZIF-67 with additional components, our work demonstrates that an enhancement in CO_2 adsorption capacity can be achieved simply by optimizing the synthesis conditions. This approach provides a cost-effective and practical strategy for improving MOF performance without the need for complex modifications. Therefore, this study evaluated the effect of synthesis conditions during the solvothermal method, including the molar ratio of salt to ligand, the molar ratio of salt to solvent, and the synthesis temperature, on the structure of ZIF-67 for CO_2 adsorption. The one-factor-at-a-time (OFAT) method was employed to optimize the synthesis of ZIF-67. In this approach, a single parameter is varied while the others are kept constant, allowing the individual effect of each factor to be clearly observed. While advanced multivariable design methods such as Design of Experiments or Response Surface Methodology can provide more comprehensive optimization, OFAT was selected here to isolate and interpret the role of each synthesis parameter. This choice is consistent with the primary objective of the present work, which was to establish a fundamental understanding of the relationship between individual synthesis factors and the CO_2 capture performance of ZIF-67. However, it should be noted that OFAT does not account for possible synergistic effects between variables (Chen et al., 2025).

2. EXPERIMENTAL

2.1. Synthesis of ZIF-67

In this research, ZIF-67 was prepared by the solvothermal method (Yang et al., 2018). Briefly, 0.291 g of $Co(NO_3)_2 \cdot 6H_2O$ (Merck) was dissolved in 15 mL of methanol (Merck). This solution was then rapidly added to 15 mL of methanol containing 0.66 g of 2-methylimidazole, which was purchased from Merck, as the ligand. Initially, the purple solution with different molar ratios of salt, ligand, and solvent was stirred for 24 hours at room temperature. Subsequently, the precipitate was collected by centrifugation at 7000 rpm for 5 minutes and washed three times with methanol. Finally, the obtained product was placed in an oven at 60 °C for 12 hours, yielding ZIF-67 powder.

2.2. Optimization of ZIF-67 structure

As previously mentioned, the OFAT method was selected for optimization. In the first step of optimization, the effect of the salt-to-ligand molar ratio was examined, while the other parameters were kept constant. For this purpose, ratios of 1:3, 1:4, 1:8, 1:12, and 1:16 were investigated. All samples were prepared at room temperature, with the salt-to-solvent molar ratio fixed at 1:741. The textural properties of the samples were compared to determine the optimum salt-to-ligand ratio. In the next step, to determine the optimum salt-to-solvent ratio, ratios of 1:494 and 1:988 were prepared under the optimized salt-to-ligand ratio at room temperature. The optimum salt-to-solvent ratio was identified by comparing the textural properties of the samples. In the final step, the effect of synthesis temperature on the formation of ZIF-67 was investigated. Two samples with the optimized salt-to-ligand and salt-to-solvent ratios were prepared at 33 °C and 43 °C to examine the influence of mild temperature variations on the crystal growth and structure of ZIF-67. These temperatures were selected as practical and convenient values within the range suitable for nucleation (Sahu et al., 2025). All of these samples were labeled and summarized in Table 1.

Table 1. Synthesis parameters for various samples

Sample	Salt: ligand: solvent molar ratios	synthesis temperature (℃)
A	1:3:741	23
B	1:4:741	23
C	1:8:741	23
D	1:12:741	23
E	1:16:741	23
F	1:4:494	23
G	1:4:988	23
H	1:4:741	33
I	1:4:741	43

2.3. Characterization

N_2 adsorption–desorption isotherms at 77 K were used to investigate the textural properties of the samples. This analysis,

known as the Brunauer–Emmett–Teller (BET) method, was carried out using a Belsorp mini II (Japan). Before performing the analysis, the samples were degassed at 100 °C for 12 hours to ensure complete removal of residual moisture. The chemical bonds of the adsorbent were determined by Fourier Transform Infrared Spectroscopy (FTIR) using a Tensor 27 (Germany) within the spectral range of 400–4000 cm^{-1}. Scanning Electron Microscopy (SEM) analysis was conducted to examine the morphology of the adsorbent surfaces, using an SEC-SNE-4500 instrument (South Korea). Thermogravimetric Analysis (TGA) was performed using a TGA 209 F1 (Germany) at 900 °C to evaluate the weight loss of the adsorbent as a function of temperature. The crystal structure of the adsorbent was studied by Powder X-ray Diffraction (PXRD), carried out using an X'Pert Pro (Netherlands) within the 2θ range of 5°–50°.

2.4. Gas adsorption system

In this research, the adsorption capacity of ZIF-67 for carbon dioxide and nitrogen storage was measured using a volumetric method in a gas adsorption system illustrated in Figure 1. The pressure cells, adsorption cells, and the main body of the apparatus were made of stainless steel with high pressure resistance. The temperature during the adsorption process was controlled using a water bath. To prevent the presence of air and unwanted gases, the system was evacuated to vacuum before starting the adsorption process. For each measurement, a specified amount of ZIF-67 (approximately 1 g) was placed in the adsorption cell. Upon opening the regulator and main valve, the gas was introduced into the pressure cell. After a short time, the input pressure was stabilized by monitoring the pressure sensor. At this stage, the connector valve was opened to allow gas to enter the adsorption cell, resulting in a pressure decrease due to gas expansion. A subsequent drop in pressure indicated the beginning of the adsorption process. When the pressure in the adsorption cell reached equilibrium, the connector valve was closed. To achieve a higher target pressure, the regulator was opened again and the above steps were repeated. The gas adsorption capacity was calculated based on the equilibrium pressures in the adsorption and pressure cells. The adsorption experiments for CO_2 and N_2 were conducted at 293, 303, and 313 K. It should be noted that ZIF-67 was regenerated by heating at 150 °C for 3.5 hours before reuse in the adsorption process.

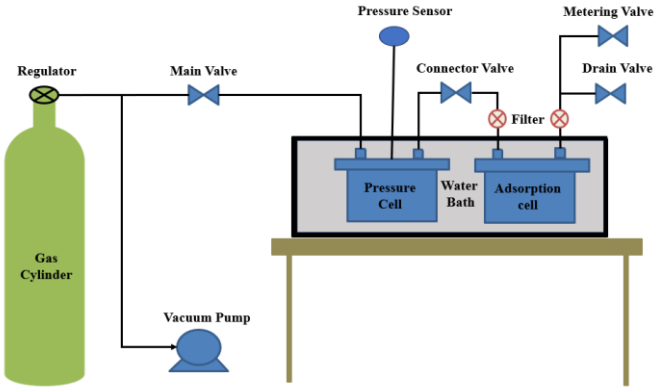

Figure 1. Schematic of gas adsorption system.

3. METHOD

3.1. Adsorption isotherms

To determine the adsorption isotherms, commonly used models such as Langmuir, Freundlich, and Langmuir–Freundlich were applied. These models describe the relationship between the amount of gas adsorbed and pressure at a constant temperature. In brief, the Langmuir model assumes monolayer adsorption, no interactions between adsorbed molecules, and identical adsorption sites for all adsorbed species. These assumptions correspond to an ideal adsorption condition. The Langmuir model is expressed by equation (1), where q_e (mmol/g) denotes the equilibrium adsorption capacity and q_m (mmol/g) represents the maximum adsorption capacity (Ahmadpari et al., 2019; Keramati & Ghoreyshi 2014). In this equation, K_L (bar $^{-1}$) and P (bar) represent the Langmuir constant and pressure, respectively.

$$q_e = q_m \frac{k_L P}{1+k_L P} \quad (1)$$

The Freundlich model is appropriate for non-ideal adsorption onto heterogeneous surfaces. In this model, the adsorption process happens in the form of a multilayer with unequal energies (Debord et al., 2023). This model follows Equation (2) where k_f (mmol/g bar$^{1/n}$) and (n) are the Freundlich constant and exponent, respectively.

$$q_e = k_f P^{1/n} \quad (2)$$

The Langmuir-Freundlich model is a combination of the two mentioned models. The advantages of this model include high adaptability with experimental isotherm and simplicity of mathematical calculations, which can be applied to modeling the behavior of different adsorbents (Agnihotri et al., 2005). This model follows Equation (3) where k_s (bar^{-1}) indicates the Langmuir-Freundlich constant. In addition, this model is converted into Langmuir isotherm for n=1.

$$q_e = q_m \frac{(k_s P)^{1/n}}{1+(k_s P)^{1/n}} \quad (3)$$

3.2. Adsorption Thermodynamic

Adsorption is generally considered an exothermic process, and the heat released during this process, known as the isosteric heat of adsorption, can be determined using the Clausius–Clapeyron equation (4) (Rehman & Park, 2017). In this equation, ΔH_{st} (kJ/mol) represents the isosteric heat, R is gas constant (R=8.314 J/mol k), and P (pa) and T (K) are introduced as the pressure and temperature, respectively.

$$\Delta H_{st} = R \left(\frac{d \ln P}{d(1/T)}\right) \quad (4)$$

3.3. CO_2/N_2 Selectivity

The adsorption affinity of gases on the adsorbent surface is represented by the selectivity factor, which plays a crucial role in the separation of gas mixtures. In gas mixtures, direct determination of selectivity for certain components can be challenging; therefore, the adsorption isotherms of individual pure gases are often used to estimate selectivity. For this purpose, the Ideal Adsorbed Solution Theory (IAST) is applied based on the adsorption isotherm data (Skopp, 2009). According to IAST, the CO_2/N_2 selectivity is described by Equation (5):

$$S_{CO_2/N_2} = \frac{x_{CO_2}/y_{CO_2}}{x_{N_2}/y_{N_2}} \quad (5)$$

where (S) is the selectivity factor; x and y are the mole fractions related to adsorbed and gas phases, respectively.

4. RESULTS AND DISCUSSION

4.1. Optimization of synthesized ZIF-67 parameters

It was expected that the optimum sample, characterized by a high surface area and a low pore diameter, would exhibit the maximum adsorption capacity. Accordingly, the effect of synthesis parameters on the adsorbent structure was investigated using BET analysis during nitrogen adsorption-desorption.

4.1.1. Evaluation of the effect of molar ratio salt/ligand

As previously mentioned, the molar ratio of salt to ligand was selected as the first key parameter. The prepared samples were analyzed using BET (Table 2). According to the data, increasing the ligand ratio from 3 to 4 (samples A to B) resulted in an increase in the specific surface area from 1700.7 to 2285 m^2/g. This trend may be attributed to improved crystallization, as a higher ligand concentration can enhance coordination with cobalt ions and promote crystal growth (Missaoui et al.,2024; Shi et al., 2017). However, at ratios higher than 4, the excess ligand likely caused incomplete dissolution in the solvent, which may have impeded crystallization and consequently reduced the surface area. As shown in Table 2, sample B exhibited the highest surface area and the smallest mean pore size among all samples. This sample, having the optimum ligand ratio, provided more active sites for gas adsorption, allowing a greater number of gas molecules to interact with the adsorbent surface and thereby enhancing the adsorption capacity (Chen et al., 2025; Lai et al., 2014).

Table 2. Textural properties of ZIF-67 samples with the different molar ratio of ligand

Sample	BET (m^2/g)	Total pore volume (cm^3/g)	Micropore volume (cm^3/g)	Mean pore diameter (nm)
A	1700.7	0.6603	0.6511	1.5531
B	2285	0.6801	0.6774	1.1906
C	2078.2	0.7044	0.6992	1.3557
D	1901.4	0.6114	0.6075	1.2862

4.1.2. Investigation of the effect of molar ratio salt/solvent

In this section, the optimum molar ratio of salt to solvent was determined by analyzing the structural properties obtained from BET measurements (Table 3). For this purpose, molar ratios of 1:494, 1:741, and 1:988 were investigated. It is worth noting that all samples were synthesized at room temperature (23 °C) using the previously optimized salt-to-ligand molar ratio of 1:4:X. According to the results, sample B was identified as the optimum sample, exhibiting the highest surface area and the smallest pore diameter among the tested samples. As the molar ratio of solvent decreased from 988 to 741, the specific surface area increased from 1840.4 m^2/g to 2285 m^2/g, respectively. This enhancement can be attributed to the higher concentration of metal ions and ligands in the reaction medium, which likely promoted nucleation and crystal growth (Lin et al., 2017; Torad et al., 2013). However, at a molar ratio lower than 741, the salt and ligand appeared to reach saturation, which may have limited proper dissolution and hindered crystal growth, leading to a reduction in the surface area (Chen et al., 2025; Migliorati et al., 2011).

Table 3. Textural properties of ZIF-67 samples with a different molar ratio of solvent

Sample	BET (m^2/g)	Total pore volume (cm^3/g)	Micropore volume (cm^3/g)	Mean pore diameter (nm)
F	1716.2	0.6543	0.6436	1.5249
B	2285	0.6801	0.6774	1.1906
G	1840.4	0.7039	0.6919	1.5298

4.1.3. Investigation of the effect of synthesis temperature

According to the results of the BET analysis, the optimum sample with the highest surface area and the lowest pore diameter was obtained at the salt, ligand, and solvent molar ratio of 1:4:741, respectively. In the two previous steps, all samples were synthesized at room temperature, while in this step, the effect of synthesis temperature was examined by preparing the samples at 33 °C and 43 °C. A comparison of the results in Table 4 demonstrated that room temperature was the most suitable condition for the synthesis of ZIF-67. As the temperature decreased from 43 °C to 23 °C, the nucleation rate and crystal growth were enhanced, resulting in the formation of more void spaces (Khoshhal et al., 2015). Therefore, room temperature was selected as the optimum synthesis temperature, and based on the investigation of the synthesis parameters of ZIF-67, the optimum molar ratio was determined to be 1:4:741.

Table 4. Textural properties of ZIF-67 samples with different synthesis temperatures

Sample	BET (m^2/g)	Total pore volume (cm^3/g)	Micropore volume (cm^3/g)	Mean pore diameter (nm)
B	2285	0.6801	0.6774	1.1906
H	1724.3	0.6564	0.6525	1.5227
I	1749.4	0.6688	0.6651	1.5293

4.2. Characterization of the optimized ZIF-67

For further evaluation of the ZIF-67 structure, various analyses were performed on the optimum sample. The textural properties of ZIF-67 were investigated using BET analysis. Figure 2a shows the nitrogen adsorption-desorption isotherm at 77 K corresponding to the optimum sample. According to this figure, the adsorption-desorption curve did not exhibit a hysteresis loop. Furthermore, it can be observed that the saturation state of the adsorbent was achieved in a short time and at low pressure (Sahu et al., 2025; Thommes et al., 2015). These results indicate that ZIF-67 possesses a microporous structure. According to the IUPAC classification, the isotherm of this sample corresponds to type I. In this type of isotherm, adsorption occurs in a monolayer on the adsorbent surface, which is characteristic of the physisorption behavior of microporous materials (Sing, 1985). Moreover, Figure 2b shows the pore diameter distribution (0–2 nm), further confirming the microporous structure of ZIF-67.

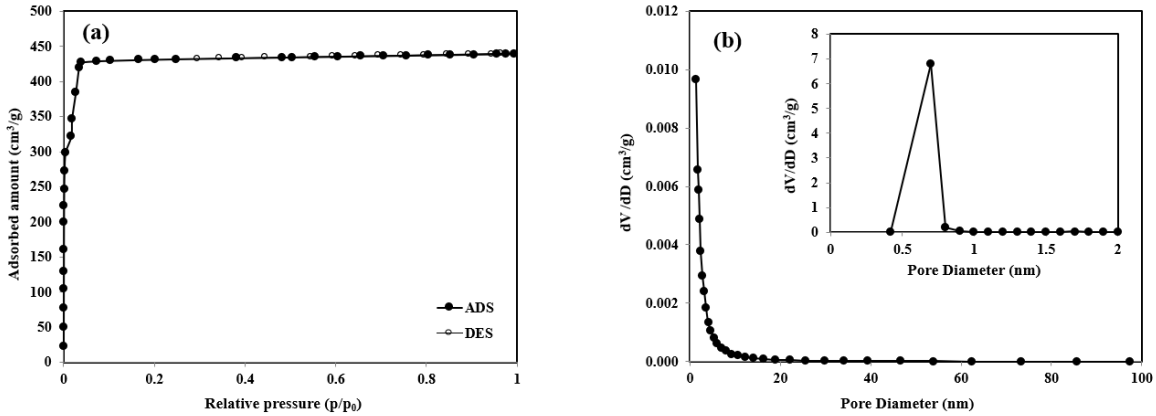

Figure 2. BET analysis of the optimized ZIF-67; (a) nitrogen adsorption- desorption and (b) the pore diameter distribution in the range of 0-2 nm and 0-100 nm.

The FTIR spectrum of ZIF-67 is shown in Figure 3a. The peak at 421.41 cm^{-1} corresponds to Co–N stretching vibrations. The bending and stretching vibrations associated with the imidazole ring are observed in the range of 600–1500 cm^{-1} (Dong et al., 2019). The peak at 1647.38 cm^{-1} corresponds to C=N bonds. Furthermore, two peaks around 2930.42 cm^{-1} and 3129.92 cm^{-1} represent the C–H stretching vibrations related to the aliphatic chain and the aromatic ring in the imidazole, respectively (He et al., 2014).

As previously mentioned, SEM analysis was employed to characterize the adsorbent morphology. SEM images of ZIF-67 are shown in Figure 3b. The images reveal that the adsorbent exhibits a rhombic dodecahedron shape, with particle sizes smaller than 500 nm. These results are in good agreement with previous studies and confirm the successful synthesis of the adsorbent (Lai et al., 2021; Shao et al., 2014).

To evaluate the thermal stability of ZIF-67, TGA analysis was performed, and the results are shown in Figure 3c. A minor weight loss observed at 100 °C is attributed to the removal of adsorbed moisture. The adsorbent remained stable up to 500 °C, while significant weight loss occurred at higher temperatures due to ligand decomposition. This high-temperature stability ensures that the adsorbent can be regenerated by heating and can undergo repeated adsorption-desorption cycles (Yang et al., 2018).

The crystal structure of ZIF-67 was characterized using PXRD analysis, shown in Figure 3d. The results are consistent with previous studies, confirming the successful synthesis of the adsorbent (Shi et al., 2011). The narrowness of all peaks indicates high crystallinity. The peak at 7.4°, corresponding to the (011) plane, is more intense than the other peaks due to favorable orientation of this plane.

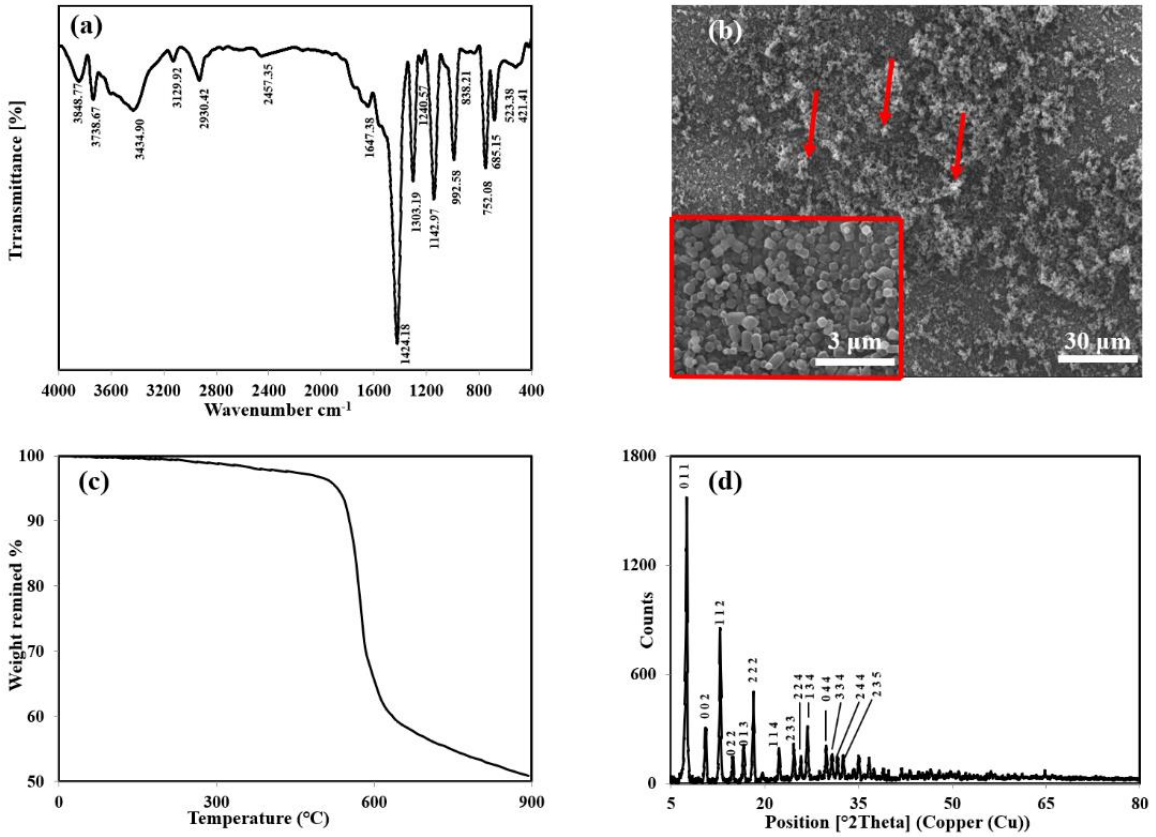

Figure 3. Characterization of the optimized ZIF-67; (a) The FTIR spectrum (b) SEM images (c) The TGA analysis (d) PXRD analysis.

4.3. The performance of adsorbent for gas adsorption

The adsorbent was initially used for CO_2 adsorption and was subsequently employed to determine the selectivity of CO_2 from flue gas by evaluating the performance of ZIF-67 for N_2 adsorption. Adsorption experiments for the two gases were conducted at 293, 303, and 313 K, with pressures selected up to 10 bar. The results for CO_2 and N_2 adsorption by ZIF-67 are depicted in Figure 4. It is evident that increasing the pressure and decreasing the temperature enhanced the gas adsorption capacity of the adsorbent. This can be attributed to the fact that increasing the pressure raises the number of gas molecules per unit volume, which enhances their likelihood of interacting with the adsorbent surface and thus promotes adsorption. In addition, increasing the pressure increases the energy of gas molecules due to more frequent collisions with the adsorbent surface, further increasing the adsorption capacity. Since adsorption is an exothermic process, a reduction in temperature also leads to an increase in adsorption capacity. The CO_2 adsorption capacity at 293 K and 10 bar was measured at 7.88 mmol/g, representing the highest adsorption capacity of ZIF-67. Under the same conditions (T = 293 K, p = 10 bar), the amount of N_2 adsorbed was 2.54 mmol/g. Comparing the results for CO_2 and N_2 adsorption indicates that ZIF-67 performs better for CO_2 adsorption. Notably, the pore aperture of ZIF-67 crystals is 0.34 nm, which lies between the kinetic diameters of CO_2 (0.33 nm) and N_2 (0.365 nm). This close size matching allows CO_2 molecules to diffuse into the micropores of ZIF-67 more readily than N_2, producing a molecular sieving effect. Furthermore, CO_2 interacts strongly with the ZIF-67 framework, resulting in higher electrostatic affinity compared with the weaker interactions of N_2 molecules (Yang et al., 2018). These combined factors at the molecular level provide a rationale for why CO_2 adsorption capacity and selectivity are consistently higher than those of N_2 (Simmons et al., 2011).

Experimental data for CO_2 and N_2 were fitted using the Langmuir (Figure 4a), Freundlich (Figure 4b), and Langmuir-Freundlich models (Figure 4c) at temperatures of 293, 303, and 313 K. As shown, the Langmuir-Freundlich model provided a better fit for both gases. The adsorption isotherms were well described by the Langmuir-Freundlich model, which may suggest the possibility of multilayer adsorption. From the shape of the isotherms, it can be inferred that at low pressures, the micropores are initially occupied by gas molecules in single layers, corresponding to Langmuir sites, followed by adsorption on larger pores in a multilayer arrangement. However, this remains a hypothesis and requires further experimental confirmation. The constants of the aforementioned equations were obtained by curve fitting in MATLAB (R2017b) and are summarized in Table 5. It can be seen that higher adsorption capacities (qm) were achieved at lower operating temperatures. In addition, increasing the temperature reduced the gas affinity for the adsorbent surface, resulting in a decrease in the "n" constant in the Freundlich isotherm (Khoshhal et al., 2015). Furthermore, owing to the high affinity of ZIF-67 for CO_2 molecules, all constants obtained for CO_2 are higher than those for N_2. According to Table 5, for both gases, the Langmuir-Freundlich model exhibited a higher correlation coefficient ($R^2 > 0.99$) compared with the other models, making it suitable for describing CO_2 and N_2 adsorption.

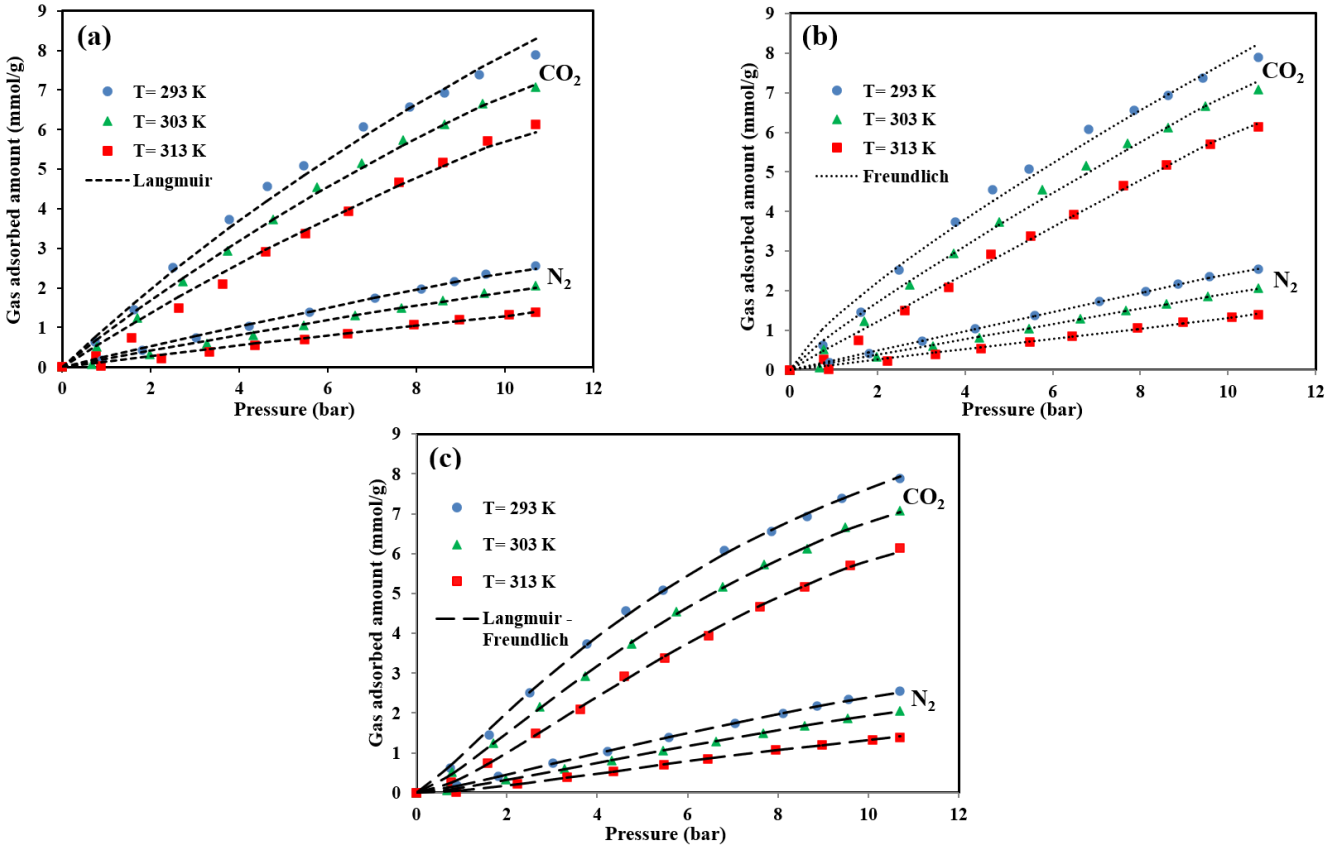

Figure 4. Fitting of experimental data for CO_2 and N_2 adsorption; (a) Langmuir, (b) Freundlich, and (c) Langmuir-Freundlich at 293, 303, 313 K.

Table 5. The constants of the three mentioned isotherm for CO_2 and N_2

		CO_2			N_2	
Temperature (K)	293	303	313	293	303	313
Langmuir						
K_L	0.0325	0.0302	0.0257	0.0134	0.0124	0.0108
q_m	32.12	29.63	27.95	20.13	17.19	13.17
R^2	0.9910	0.9965	0.9888	0.9973	0.9921	0.9850
Freundlich						
K_F	1.283	0.934	0.617	0.247	0.195	0.131
n	1.275	1.145	1.016	1.009	1.005	1.002
R^2	0.9882	0.9929	0.9959	0.9991	0.9971	0.9910
Langmuir-Freundlich						
K_S	0.1093	0.1037	0.1012	0.0468	0.0631	0.0867
n	0.8289	0.7614	0.6746	0.8251	0.7332	0.6425
q_m	14.51	13.32	11.59	8.43	5.56	2.96
R^2	0.9990	0.9996	0.9990	0.9996	0.9995	0.9995

As illustrated in Table 6, the performance of the synthesized ZIF-67 demonstrated a higher adsorption capacity compared with some previous studies. In this work, this was achieved by adjusting the synthesis conditions without performing complex experimental steps, which significantly facilitates the scale-up of the nanomaterials. This strategy represents a key highlight of the study.

Table 6. Comparison of CO_2 adsorption capacity onto different adsorbents at ~1 bar.

Adsorbent	Adsorption capacity (mmol/g)	Adsorption temperature (k)	References
ZIF-67	0.65	303	(Yang et al., 2018)
LDH@ZIF-67	0.50	303	(Yang et al., 2018)
SOD-ZIF-67	2.08	298	(Missaoui et al., 2024)
ZIF-8	0.53	298	(Lai et al., 2014)
ZIF-67/ chitosan	1.21	273	(Hammi et al., 2023)
Ni@ZIF-67	0.76	273	(Bheeram et al., 2023)
ZIF-67	0.94	293	This Work

4.4. Adsorption Thermodynamic

The isosteric heat of CO_2 and N_2 adsorption was obtained using the Clausius–Clapeyron equation, with calculations performed under the assumption of constant adsorption capacity. Figure 5 illustrates the isosteric heat of the two gases. As shown, the isosteric heat decreased with increasing adsorption capacity. This reduction indicates that the adsorption sites on the surface of the adsorbent are heterogeneous and suggests the possible occurrence of multilayer adsorption (Yan et al., 2013). These results imply that as adsorption capacity increases, the interaction between the gas and the adsorbent decreases, leading to a lower isosteric heat. Notably, the isosteric heat of CO_2 adsorption is higher than that of N_2 adsorption. For ease of curve plotting, the isosteric heat is presented as an unsigned quantity. It is reported here as a positive value, representing the magnitude of the exothermic interaction between gas molecules and the adsorbent framework (Li et al., 2025). It is worth noting that an isosteric heat below 40 kJ/mol indicates physisorption. Therefore, according to Figure 5, the dominant mechanism for CO_2 and N_2 adsorption by ZIF-67 is physisorption.

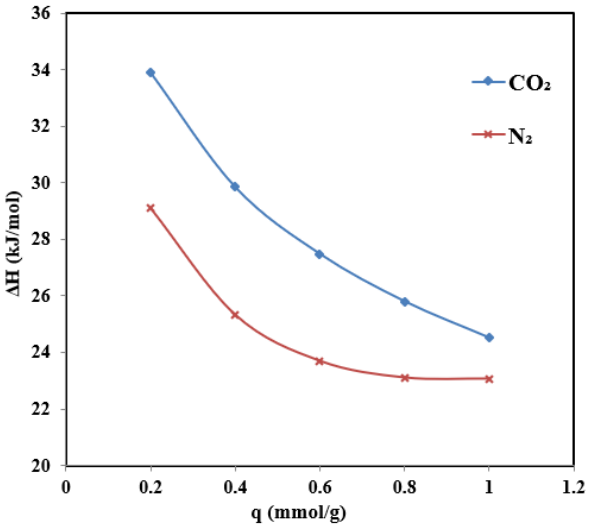

Figure 5. Isosteric heat of CO_2 and N_2 adsorption

4.5. Determination of selectivity and regeneration of ZIF-67

As previously stated, the adsorbent was used for CO_2 and N_2 adsorption separately. Considering that flue gas contains a mixture of 15% CO_2 and 85% N_2, it is necessary to determine the CO_2/N_2 selectivity. Since the adsorption isotherms of the two gases were fitted using the Langmuir-Freundlich equation, the constants from this model were employed to calculate selectivity. The calculations were performed at 293, 303, and 313 K, and the results are shown in Figure 6a. According to this figure, the highest selectivity observed was 5.86 at 313 K and 1 bar. The increase in CO_2/N_2 selectivity with temperature can be explained by the energetic difference between CO_2 and N_2 adsorption, as shown in Figure 5. The isosteric heat of CO_2 adsorption is consistently higher than that of N_2 across the studied loading range, indicating stronger energetic interactions between CO_2 (with high polarizability and a large quadrupole moment) and the ZIF-67 framework compared with N_2 (Li et al., 2025). Consequently, although both gases exhibited a decrease in adsorption capacity at elevated temperatures, CO_2 showed a relatively smaller loss in adsorption compared to N_2 (Table 5). These results suggest that the synthesized adsorbent can effectively manage CO_2 separation from flue gas.

Considering economic and environmental factors, adsorbent recyclability is an important parameter for evaluating performance. The adsorbent should maintain its adsorption capacity after multiple adsorption-desorption cycles (Zhang et al., 2014). In this study, ZIF-67 was regenerated by heating and subjected to several adsorption-desorption cycles. After five cycles, its performance for CO_2 adsorption was evaluated. The results in Figure 6b show that the adsorption capacity decreased slightly from 8.46 to 7.88 mmol/g. This minor reduction, corresponding to more than 93% regeneration efficiency, demonstrates that the optimized ZIF-67 is a promising candidate for CO_2 adsorption applications.

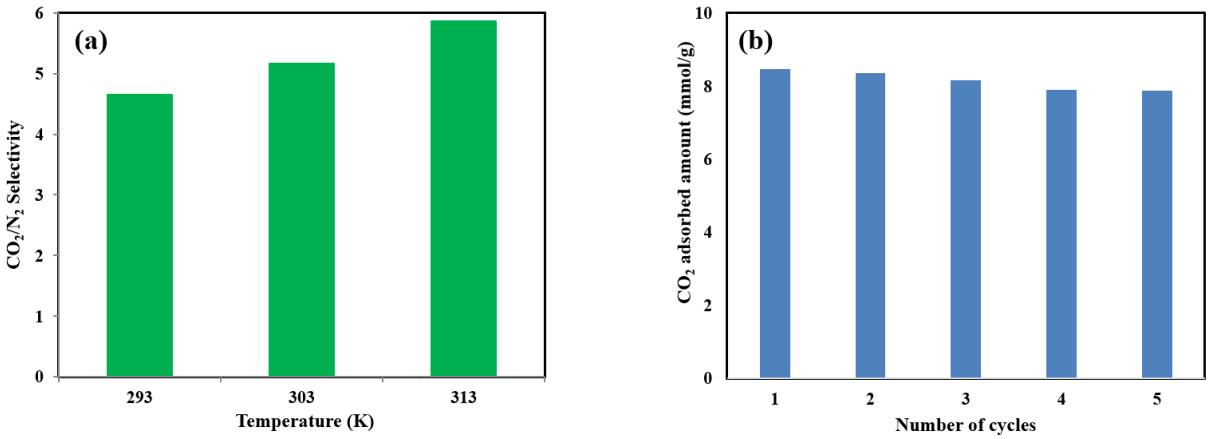

Figure 6. (a) CO_2/N_2 Selectivity at 293, 303, 313 K (b) CO_2 adsorption capacity after five cycles

5. CONCLUSIONS

In this study, ZIF-67 was synthesized under various conditions by adjusting synthesis parameters such as salt, ligand, solvent, and temperature to enhance its performance for CO_2 capture. The optimized conditions produced ZIF-67 with an enhanced surface area (2285 m^2/g), which contributed to a higher CO_2 adsorption capacity (0.94 mmol/g at 293 K and 1 bar), comparable to values reported for similar ZIF-based adsorbents. The adsorption data were best described by the Langmuir–Freundlich model ($R^2 > 0.99$), indicating the presence of heterogeneous adsorption sites and stronger interactions of CO_2 with the framework compared to N_2, as supported by the isosteric heat analysis. The CO_2/N_2 selectivity (5.86 at 313 K and 1 bar) reflected the preferential interaction of CO_2 with the ZIF-67 framework. Finally, the optimized ZIF-67 retained more than 93% of its adsorption efficiency, demonstrating a feature suitable for industrial applications. Overall, these findings indicate that adjusting the synthesis conditions of ZIF-67 is a simple and cost-effective strategy to improve its efficiency as a solid adsorbent for CO_2 capture; however, further optimization is required to advance its application in large-scale carbon capture systems.

ACKNOWLEDGEMENT

This work was supported by the Oil Lab of Babol Noshirvani University of Technology.

REFERENCES

1. Agnihotri, S., Rood, M. J., & Rostam-Abadi, M. (2005). Adsorption equilibrium of organic vapors on single-walled carbon nanotubes. *Carbon*, *43*(11), 2379-2388. https://doi.org/10.1016/j.carbon.2005.04.020
2. Ahmadpari, H., Noghany, M. E., Ladez, B. R., Mehrparvar, B., & Momeni, S. (2019). Kinetics modeling and isotherms for adsorption of nitrate from aqueous solution by wheat straw. Tecnologia e Ambiente, 25, 203-214. https://doi.org/10.18616/ta.v25i0.5301
3. Ahmed, S., Ramli, A., & Yusup, S. (2017). Development of polyethylenimine-functionalized mesoporous Si-MCM-41 for CO_2 adsorption. *Fuel Processing Technology*, *167*, 622-630. https://doi.org/10.1016/j.fuproc.2017.07.036
4. Anbia, M., & Hoseini, V. (2012). Development of MWCNT@ MIL-101 hybrid composite with enhanced adsorption capacity for carbon dioxide. *Chemical Engineering Journal*, *191*, 326-330. https://doi.org/10.1016/j.cej.2012.03.025
5. Bheeram, V. R., Dadhich, A. S., & Mukkamala, S. B. (2023). Rapid room temperature synthesis and CO_2 uptake performance of nanocrystalline ZIF-67 and Ni@ ZIF-67. *Inorganic Chemistry Communications*, *150*, 110455. https://doi.org/10.1016/j.inoche.2023.110455
6. Chen, J., Tang, M., Nie, S., Xiao, P., Zhao, T., & Chen, Y. (2025). Synthesis Methods, Performance Optimization, and Application Progress of Metal–Organic Framework Material MIL-101 (Cr). *Chemistry*, *7*(3), 78. https://doi.org/ https://doi.org/10.3390/chemistry7030078
7. Debord, J., Chu, K. H., Harel, M., Salvestrini, S., & Bollinger, J. C. (2023). Yesterday, today, and tomorrow. Evolution of a sleeping beauty: The Freundlich isotherm. *Langmuir*, *39*(8), 3062-3071. https://doi.org/10.1021/acs.langmuir.2c03105
8. Dong, Y., Duan, C., Sheng, Q., & Zheng, J. (2019). Preparation of Ag@ zeolitic imidazolate framework-67 at room temperature for electrochemical sensing of hydrogen peroxide. *Analyst*, *144*(2), 521-529. https://doi.org/10.1039/C8AN01641K
9. Fairen-Jimenez, D., Moggach, S., Wharmby, M. T., Wright, P. A., Parsons, S., & Duren, T. (2011). Opening the gate: framework flexibility in ZIF-8 explored by experiments and simulations. *Journal of the American Chemical Society*, *133*(23), 8900-8902. https://doi.org/10.1021/ja202154j
10. Férey, G. (2009). Some suggested perspectives for multifunctional hybrid porous solids. *Dalton Transactions*(23), 4400-4415. https://doi.org/10.1039/B817360P
11. Hammi, N., Couzon, N., Loiseau, T., Volkringer, C., El Kadib, A., Royer, S., & Dhainaut, J. (2023). Hierarchically porous ZIF-67/chitosan beads with high surface area and strengthened mechanical properties: Application to CO_2 storage. *Materials Today Sustainability*, *22*, 100394. https://doi.org/10.1016/j.mtsust.2023.100394
12. He, M., Yao, J., Liu, Q., Wang, K., Chen, F., & Wang, H. (2014). Facile synthesis of zeolitic imidazolate framework-8 from a concentrated aqueous solution. *Microporous and Mesoporous Materials*, *184*, 55-60. https://doi.org/10.1016/j.micromeso.2013.10.003
13. Keramati, M., & Ghoreyshi, A. A. (2014). Improving CO2 adsorption onto activated carbon through functionalization by chitosan and triethylenetetramine. *Physica E: Low-dimensional systems and nanostructures*, *57*, 161-168. https://doi.org/10.1016/j.physe.2013.10.024
14. Khoshhal, S., Ghoreyshi, A. A., Jahanshahi, M., & Mohammadi, M. (2015). Study of the temperature and solvent content effects on the structure of Cu–BTC metal organic framework for hydrogen storage. *RSC advances*, *5*(31), 24758-24768. https://doi.org/10.1039/C5RA01890K
15. Kim, J., Lin, L.-C., Swisher, J. A., Haranczyk, M., & Smit, B. (2012). Predicting large CO_2 adsorption in aluminosilicate zeolites for postcombustion carbon dioxide capture. *Journal of the American Chemical Society*, *134*(46), 18940-18943. https://doi.org/10.1021/ja309818u
16. Lai, J. Y., Ngu, L. H., & Hashim, S. S. (2021). A review of CO_2 adsorbents performance for different carbon capture technology processes conditions. *Greenhouse Gases: Science and Technology*, *11*(5), 1076-1117. https://doi.org/10.1002/ghg.2112
17. Lai, L. S., Yeong, Y. F., Ani, N. C., Lau, K. K., & Shariff, A. M. (2014). Effect of synthesis parameters on the formation of zeolitic imidazolate framework 8 (ZIF-8) nanoparticles for CO_2 adsorption. *Particulate Science and Technology*, *32*(5), 520-528. https://doi.org/10.1080/02726351.2014.920445
18. Li, C., Yang, Z., Luo, H., Yang, T., Tong, L., Yuan, Y., ... & Xiao, J. (2025). Analytical and numerical estimations of isosteric heat of adsorption with application to hydrogen purification. *Fuel*, *381*, 133398. https://doi.org/10.1016/j.fuel.2024.133398
19. Lin, Y., Kong, C., Zhang, Q., & Chen, L. (2017). Metal-organic frameworks for carbon dioxide capture and methane storage. *Advanced*

Energy Materials, *7*(4), 1601296. https://doi.org/10.1002/aenm.201601296
20. Migliorati, V., Chillemi, G., & D'Angelo, P. (2011). On the solvation of the Zn^{2+} ion in methanol: a combined quantum mechanics, molecular dynamics, and EXAFS approach. *Inorganic Chemistry*, *50*(17), 8509-8515. https://doi.org/10.1021/ic201100q
21. Myers, A. L., & Prausnitz, J. M. (1965). Thermodynamics of mixed-gas adsorption. *AIChE Journal*, *11*(1), 121-127. https://doi.org/10.1002/aic.690110125
22. Missaoui, N., Chrouda, A., Bourguiba, F., & Serafin, J. (2024). Impact of metal precursor and molar ratios on adsorption and separation of CO_2 and CH_4 by SOD-ZIF-67 prepared using green solvent-free synthesis. *Fuel*, *378*, 132840. https://doi.org/10.1016/j.fuel.2024.132840
23. Olajire, A. A. (2010). CO_2 capture and separation technologies for end-of-pipe applications–A review. *Energy*, *35*(6), 2610-2628. https://doi.org/10.1016/j.energy.2010.02.030
24. Rehman, A., & Park, S.-J. (2017). Facile synthesis of nitrogen-enriched microporous carbons derived from imine and benzimidazole-linked polymeric framework for efficient CO_2 adsorption. *Journal of CO2 Utilization*, *21*, 503-512. https://doi.org/10.1016/j.jcou.2017.08.016
25. Sahu, B., Sanwaria, S., Singh, A. K., Patel, J., & Jugade, R. (2025). Ambient temperature fabrication of ZIF-67 MOF: A Robust UV-activated photocatalyst for dye degradation. *Journal of Molecular Structure*, *1327*, 141152. https://doi.org/10.1016/j.molstruc.2024.141152
26. Shao, J., Wan, Z., Liu, H., Zheng, H., Gao, T., Shen, M., Qu, Q., & Zheng, H. (2014). Metal organic frameworks-derived Co_3O_4 hollow dodecahedrons with controllable interiors as outstanding anodes for Li storage. *Journal of Materials Chemistry A*, *2*(31), 12194-12200. https://doi.org/10.1039/C4TA01966K
27. Shi, Q., Chen, Z., Song, Z., Li, J., & Dong, J. (2011). Synthesis of ZIF-8 and ZIF-67 by steam-assisted conversion and an investigation of their tribological behaviors. *Angewandte Chemie International Edition*, *50*(3), 672-675. https://doi.org/10.1002/anie.201004937
28. Shi, Z., Yu, Y., Fu, C., Wang, L., & Li, X. (2017). Water-based synthesis of zeolitic imidazolate framework-8 for CO_2 capture. *RSC advances*, *7*(46), 29227-29232. https://doi.org/10.1039/C7RA04875K
29. Simmons, J. M., Wu, H., Zhou, W., & Yildirim, T. (2011). Carbon capture in metal–organic frameworks—a comparative study. *Energy & Environmental Science*, *4*(6), 2177-2185. https://doi.org/10.1039/C0EE00700E
30. Sing, K. S. (1985). Reporting physisorption data for gas/solid systems with special reference to the determination of surface area and porosity (Recommendations 1984). *Pure and Applied Chemistry*, *57*(4), 603-619. https://doi.org/10.1351/pac198557040603
31. Skopp, J. (2009). Derivation of the Freundlich adsorption isotherm from kinetics. *Journal of chemical education*, *86*(11), 1341. https://doi.org/10.1021/ed086p1341
32. Thommes, M., Kaneko, K., Neimark, A. V., Olivier, J. P., Rodriguez-Reinoso, F., Rouquerol, J., & Sing, K. S. (2015). Physisorption of gases, with special reference to the evaluation of surface area and pore size distribution (IUPAC Technical Report). *Pure and applied chemistry*, *87*(9-10), 1051-1069. https://doi.org/10.1515/pac-2014-1117
33. Torad, N. L., Hu, M., Kamachi, Y., Takai, K., Imura, M., Naito, M., & Yamauchi, Y. (2013). Facile synthesis of nanoporous carbons with controlled particle sizes by direct carbonization of monodispersed ZIF-8 crystals. *Chemical Communications*, *49*(25), 2521-2523. https://doi.org/10.1039/C3CC38955C
34. Wang, F., Tan, Y.-X., Yang, H., Zhang, H.-X., Kang, Y., & Zhang, J. (2011). A new approach towards tetrahedral imidazolate frameworks for high and selective CO_2 uptake. *Chemical Communications*, *47*(20), 5828-5830. https://doi.org/10.1039/C1CC10829H
35. Wei, R., Zhao, T., Xu, H., & Gao, J. (2025). Recent Advances and Challenges of Metal-Organic Frameworks for CO2 Capture. *Dalton Transactions*. https://doi.org/10.1039/D5DT00204D
36. Yamasaki, A. (2003). An overview of CO_2 mitigation options for global warming—emphasizing CO_2 sequestration options. *Journal of Chemical Engineering of Japan*, *36*(4), 361-375. https://doi.org/10.1252/jcej.36.361
37. Yan, X., Komarneni, S., & Yan, Z. (2013). CO_2 adsorption on Santa Barbara Amorphous-15 (SBA-15) and amine-modified Santa Barbara Amorphous-15 (SBA-15) with and without controlled microporosity. *Journal of Colloid and Interface Science*, *390*(1), 217-224. https://doi.org/10.1016/j.jcis.2012.09.038
38. Yang, Y., Yan, X., Hu, X., Feng, R., Zhou, M., & Cui, W. (2018). Development of zeolitic imidazolate framework-67 functionalized Co-Al LDH for CO_2 adsorption. *Colloids and Surfaces A: Physicochemical and Engineering Aspects*, *552*, 16-23. https://doi.org/https://doi.org/10.1016/j.colsurfa.2018.05.014
39. Zhang, Z., Yao, Z.-Z., Xiang, S., & Chen, B. (2014). Perspective of microporous metal–organic frameworks for CO_2 capture and separation. *Energy & Environmental Science*, *7*(9), 2868-2899. https://doi.org/10.1039/C4EE00143E
40. Zhao, G., Wang, K., Fan, X., Yang, S., Cui, P., Yin, S., Zhong, L., Zheng, F., & Wang, Y. (2025). A facile amino ligand exchange strategy to enhance the CO2 selective adsorption capability of ZIF-67. *Separation and Purification Technology*, 134955. https://doi.org/10.1016/j.seppur.2025.134955